

# OPTIMAL CONTINUOUS-THRUST TRAJECTORIES VIA VISUAL TRADE SPACE EXPLORATION

**Daniel D. Jordan**<sup>\*</sup>  
**David B. Spencer**<sup>†</sup>  
**Timothy W. Simpson**<sup>‡</sup>  
**Michael A. Yukish**<sup>§</sup>  
**Gary M. Stump**<sup>\*\*</sup>

Engineering design problems often contain correlations and tradeoffs that may or may not be obvious or well-understood. As design problem complexity increases, decision makers find it more and more difficult to grasp these tradeoffs effectively. The rapid growth of computing power now allows the simulation of millions of design alternatives, and the ability to effectively visualize these alternatives and understand the tradeoffs associated with them has never been more important. Trade space visualization tools are designed to aid decision makers by allowing them to effectively explore a design space and grasp the underlying tradeoffs and nuances particular to their specific problem. These tools provide great potential in evaluating complex dynamical systems in the aerospace industry, among others. In this paper, we apply our trade space visualization software, the Applied Research Lab Trade Space Visualizer (ATSV), to search for optimal constant acceleration orbit transfers. This problem is formulated as a multiobjective optimization problem where it is desirable to explore various competing objectives. We identify a known optimal solution and explore the input space to search for other optimal or near-optimal trajectories. Significantly perturbing the known solution to an example problem has demonstrated that the optimal solution can be converged upon successfully.

## INTRODUCTION

Complex design can be considered a decision-making process, where a classical approach to the optimal decision process can be described by [1]:

- Identify options

---

<sup>\*</sup> Graduate Research Assistant, Department of Aerospace Engineering, The Pennsylvania State University, 229 Hammond Bldg., University Park, PA 16802 USA

<sup>†</sup> Associate Professor, Department of Aerospace Engineering, The Pennsylvania State University, 229 Hammond Bldg., University Park, PA 16802 USA; Senior Member, AAS; Associate Fellow, AIAA.

<sup>‡</sup> Professor of Mechanical and Industrial Engineering, 314D Leonhard Building, The Pennsylvania State University, University Park, PA 16802 USA; Associate Fellow, AIAA.

<sup>§</sup> Head, Product and Process Division, Applied Research Laboratory, State College, PA 16804 USA

<sup>\*\*</sup> Research Assistant, Applied Research Laboratory, State College, PA 16804 USA

- Identify ways to evaluate options
- Weight each evaluation dimension
- Do the rating
- Pick the option with the highest score

This method, *rational choice analyses*, is taught in engineering and business curriculums. With this approach, rational choices are made after applying game-theoretic or statistical-theoretic methods to a problem [2]. Within the visualization community, interactive optimization-based design methods fall mainly into the category of computational steering whereby the user (i.e., designer) interacts with a simulation during the optimization process to help “steer” the search process toward what looks like an optimal solution. The steering process allows the designer to gain new perspectives on correlations within the problem and use intuition, heuristics, or some other method to adjust the design space to move towards solutions that they feel are promising. On the importance of visualization in engineering optimization, Messac and Chen [3] noted: “If effectively exploited, visualizing the optimization process in real time can greatly increase the effectiveness of practical engineering optimization.” Furthermore, Ng [4] advocates the use of data visualization and interaction to support the designer in making informed decisions and tradeoffs during multiobjective optimization. Many others argue that visualization should be considered a solution tool and that “human-in-the-loop” optimization has significant advantages over black-box search algorithms [5]-[6].

The Applied Research Lab Trade Space Visualizer (ATSV)<sup>\*</sup> used in this research has been developed to support the exploration phase of the design process by offering the following functionality [7]:

1. Visualize complex datasets using multi-dimensional visualization techniques
2. Assign variables to glyph, histogram, and parallel coordinates plots
3. Specify upper and lower bounds of an n-dimensional design space
4. Implement dynamic brushing within glyph, parallel coordinates, and histogram plots to uncover relationships in the dataset (linked views)
5. Visualize different regions of interest, using preference shading and corresponding Pareto frontier identification
6. Implement visual steering commands to navigate multi-attribute trade spaces via various Attractor/Pareto Samplers
7. Create multiple views of glyph, histogram, and parallel coordinates plots of the same trade space
8. Select a design from the glyph plot to display quantitative information, 3D geometries, and other files such as images and documents
9. Use advanced visualization hardware to view graphs and 3D geometries in stereo mode

This software has been implemented for the optimization of various multi-objective problems including orbital mechanics applications, although all functions are not used. The ATSV's exploration capabilities have been previously applied to a simple impulsive

---

<sup>\*</sup> "Applied Research Laboratory Trade Space Visualization", <http://www.atsv.psu.edu>, date cited 1/01/09.

orbit transfer to test its effectiveness on a simple dynamic problem with a known optimal solution [8]. In this work we apply the exploration and visual steering capabilities of our software to the more complex problem formulation of continuous-thrust orbital transfers.

## **ATSV BACKGROUND**

The ATSV can explore design spaces statically or dynamically. Static data sets are text or spreadsheet files generated from an external model in which decision variables and objective function values for each solution are organized. Dynamic datasets more fully utilize the potential of the ATSV by integrating visual steering into the exploration process [9]. Visual steering can be defined as the process of observing a global search and making adjustments to it in real time as the designer sees fit [6]. It allows the designer to simultaneously explore the trade space and exploit new information and insights as they are gained.

Currently, the ATSV has the ability to specify five types of visual steering commands to generate new data by random sampling, manual sampling, attractor-based sampling, preference-based sampling, and Pareto sampling. More details on these sampling methods are discussed in Reference [6]. The ATSV's attractor based sampling creates points in the objective space close to a desired location, specified by an "attractor".

A Pareto-modified evolutionary algorithm, specifically Differential Evolution [10], is used to guide the sampling process for the attractor, Pareto, and preference samplers in order to generate points in the objective space from  $n$ -dimensional discrete and continuous inputs. Details on the implementation of Pareto-modified Differential Evolution and the visual steering commands within ATSV can be found in Ref. [9].

The ability of the user to “guide” an evolution process is a recently developed addition to the Pareto sampler. Guided Pareto Sampling allows the user to choose solutions they wish to start or continue an evolution process. This gives the decision maker the advantage of influencing an evolution as it progresses with his/her intuition or knowledge gained from current and/or previous visualizations and evolution processes. Guided Pareto Sampling with an example of its application is discussed further in the Results and Discussion section.

## **LOW-THRUST ORBITAL MANEUVERS**

A spacecraft in orbit can be defined by a set of six orbital elements which describe its orientation in space. The classical orbital elements (semi-major axis  $a$ , eccentricity  $e$ , inclination  $i$ , right ascension of the ascending node  $\Omega$ , argument of periapsis  $\omega$ , and true anomaly  $\theta$ ) describe the size ( $a$ ) and shape ( $e$ ) as well as the orientation ( $i$ ,  $\Omega$ ,  $\omega$ ) of the orbit. The sixth element ( $\theta$ ) describes the angular position of the spacecraft on the particular orbit described by the previous five elements.

In order to avoid the singularities associated with the classical orbital elements for circular and/or non-inclined orbits, equinoctial orbital elements ( $a$ ,  $h$ ,  $k$ ,  $p$ ,  $q$ ,  $L$ ) are used in the derivation of the equations of motion [11]. The simple transformation, shown in Eq. 1, eliminates all singularities except for the retrograde orbit with  $i = 180^\circ$ .

<i>Classical to Equinoctial</i>	<i>Equinoctial to Classical</i>	
$a = a$	$a = a$	
$h = e \sin(\omega + \Omega)$	$e = (h^2 + k^2)^{1/2}$	
$k = e \cos(\omega + \Omega)$	$i = 2 \tan^{-1} \left( \sqrt{p^2 + q^2} \right)$	
$p = \tan(i/2) \sin(\Omega)$	$\Omega = \tan^{-1}(p/q)$	(1)
$q = \tan(i/2) \cos(\Omega)$	$\omega = \tan^{-1}(h/k) - \tan^{-1}(p/q)$	
$L = \theta + \omega + \Omega$	$\theta = L - \tan^{-1}(h/k)$	

Edelbaum et al., [12] using the calculus of variations, developed the equations of motion describing how a spacecraft's equinoctial orbital elements change with time due to an applied thrust. A set of these equations, modified by Kechichian [13], are shown as

$$\dot{\bar{x}}_e = f_t[M] \bar{u} + n \bar{e}_L \quad (2)$$

$$\dot{\bar{\lambda}} = \frac{\partial H}{\partial \bar{x}_e} = -\bar{\lambda}^T \frac{\partial [M]}{\partial \bar{x}_e} \bar{u} f_t - \lambda_L \frac{\partial n}{\partial \bar{x}_e} \quad (3)$$

where  $\bar{e}_L = (0 \ 0 \ 0 \ 0 \ 0 \ 1)^T$ , which means it is a unit vector in the direction of  $L$ .

The equinoctial element state vector  $\bar{x}_e$  and its derivative  $\dot{\bar{x}}_e$ , as well as the adjoint variable state vector (Lagrange multiplier)  $\bar{\lambda}$  and its derivative  $\dot{\bar{\lambda}}$  are respectively defined as

$$\bar{x}_e = \begin{bmatrix} a \\ h \\ k \\ p \\ q \\ L \end{bmatrix} \quad \dot{\bar{x}}_e = \begin{bmatrix} \dot{a} \\ \dot{h} \\ \dot{k} \\ \dot{p} \\ \dot{q} \\ \dot{L} \end{bmatrix} \quad \bar{\lambda} = \begin{bmatrix} \lambda_a \\ \lambda_h \\ \lambda_k \\ \lambda_p \\ \lambda_q \\ \lambda_L \end{bmatrix} \quad \dot{\bar{\lambda}} = \begin{bmatrix} \dot{\lambda}_a \\ \dot{\lambda}_h \\ \dot{\lambda}_k \\ \dot{\lambda}_p \\ \dot{\lambda}_q \\ \dot{\lambda}_L \end{bmatrix} \quad (4)$$

The matrix  $[M]$  is a  $6 \times 3$  matrix containing expressions involving partial derivatives of each state element in  $\bar{x}_e$ ; further information regarding the definition of  $[M]$  can be found in Refs. [13]-[14]. The vector  $\bar{u}$  is a unit vector pointing in the thrust direction,

$$\bar{u} = \frac{[M]^T \bar{\lambda}}{\|[M]^T \bar{\lambda}\|} \text{ where } \begin{bmatrix} u_f = \cos \alpha \cos \beta \\ u_g = \sin \alpha \cos \beta \\ u_w = \sin \beta \end{bmatrix} \quad (5)$$

The angles  $\alpha$  and  $\beta$  are yaw (in plane) and pitch (out-of-plane) angles respectively, and  $f_t$  is the constant applied acceleration. There are no coasting arcs, meaning  $f_t$  is constant and positive for all time  $t$ . The mean motion  $n$  is given by  $n = (\mu / a^3)^{1/2}$  where  $\mu$  is the gravitational parameter. The scalar Hamiltonian for this system is defined as

$$H = \bar{\lambda}^T [M] \bar{u} f_t + \lambda_L \bar{e}_L \quad (6)$$

where the end condition,  $H = 1.0$ , corresponds to the minimum-time minimum-fuel transfer.

In this paper, constant acceleration transfers are explored. The equinoctial state  $\bar{x}_e$  and the adjoint variable state  $\bar{\lambda}$  are modified to include spacecraft mass  $m$  and an associated Lagrange multiplier  $\lambda_m$  respectively. The formerly constant applied acceleration  $f_t$  is replaced with the definition

$$f_t = T / m \quad (7)$$

where  $T$  is the constant applied thrust and  $m$  is the instantaneous spacecraft mass.

## Previous Work

Some of the earliest to explore optimizing low-thrust trajectories using the variation of parameter equations to model orbital perturbations with equinoctial elements as well as

adjoint variables were presented by Edelbaum et al [12]. Due to the limited computing power at that time, averaging of the state and adjoint equations of motion was employed to allow reasonable computation time. Kechichian explored a similar problem using precision-integration of the equations of motion and compared the results to Edelbaum's averaging technique; the accuracy differences between the two techniques were significant [13]. In his work, the initial adjoint variables were optimized using an iterative scheme based on a general descent method, where the aim was to optimize an objective function consisting of a weighted sum of the differences between the actual and desired final orbit properties. The result was an optimized set of initial adjoint variables that correspond to the control angle time histories which creates the minimum-time minimum-fuel trajectory (assumes no coast arcs) from LEO to GEO for  $f_t = 9.8 \times 10^{-5}$  km/s<sup>2</sup>, as shown in Table 1.

**Table 1: Optimal Initial Adjoint Variables for LEO to GEO Transfer Found by Kechichian [13]**

Adjoint Variable	Initial Value
$\lambda_{a,o}$	1.260484756 sec/km
$\lambda_{h,o}$	386.5626962 sec
$\lambda_{k,o}$	-9388.262635 sec
$\lambda_{p,o}$	-2277.132367 sec
$\lambda_{q,o}$	-17430.27218 sec
$\lambda_{L,o}$	515.5487187 sec/rad
$H$	1.002694
$TOF$	58624.094 s

More recently, the problem has been revisited by Igarashi [14] in the attempt to search specific bounds ( $\pm 5\%$ ,  $\pm 10\%$ ,  $\pm 20\%$ ) on the set of known optimal initial adjoint variables using a variety of evolutionary algorithms. The results found in Igarashi's work closely matched those found by Kechichian.

Here, we revisit this problem once again using an evolutionary algorithm, specifically Differential Evolution, which has been integrated into ATSV. The bounds on the known optimal initial adjoint variables will be extended beyond what was explored by Igarashi in the attempt to find other optimal or near-optimal solutions. Qualitative observations are made on the effectiveness of the integration of the user/designer into the real-time visualization and multi-objective optimization elements of ATSV.

### Problem Specification

The orbit transfer between the low-Earth orbit specified in Table 2 (a) and the geosynchronous orbit specified Table 2 (b) is the transfer of interest for this work – identical to the transfer explored in Refs. [13]-[14].

**Table 2: (a) Initial LEO “Baseline” Orbit Characteristics and (b) Final GEO Orbit Characteristics**

(a) Initial Low-Earth Orbit		(b) Final Desired Orbit	
$a_o$	7000 (km)	$a_{desired}$	42000 (km)
$e_o$	0	$e_{desired}$	0.001
$i_o$	28.5°	$i_{desired}$	1°
$\Omega_o$	0°	$\Omega_{desired}$	0°
$\omega_o$	0°	$\omega_{desired}$	0°
$\theta_o$	-220°	$\theta_{desired}$	Free

For the constant acceleration problem described in the previous section, the initial conditions of the equinoctial state  $\bar{x}_{e_o}$  are known but the initial conditions of the adjoint variables  $\bar{\lambda}_o$  are unknown. Therefore, the decision space consists of the initial conditions of these six adjoint variables. Given  $\bar{\lambda}_o$  and  $f_i$  ( $f_i = 9.8 \times 10^{-5} \text{ km/s}^2$ ), Eqs. (2) and (3) are simultaneously integrated using the *ODE45* function in MATLAB. At the termination of

integration, the states of interest are the final equinoctial state  $\bar{x}_{e,f}$  and the Hamiltonian  $H$  of the system.

The objectives are to achieve the desired final orbit  $\bar{x}_{e,desired}$  and minimize time of flight via the transversality condition  $H = 1.0$ . This “target oriented” objective is transformed into a “goal oriented” objective by considering the minimization of a weighted sum of absolute differences between the final state and the desired final state, as shown in Eq. (8). The two objectives can only be lumped together in a cost function because the problem formulation ensures that they do not compete. Reaching the final desired orbit is a fundamental objective, but the minimization of time of flight is an objective with a preference. Since trajectories that do not reach GEO are not viable, the minimization of time of flight cannot compete with it. Note that the weights and the order of magnitude of the terms comprising  $f$  can significantly affect the ability of a search algorithm to properly converge to an optimal solution.

$$f = w_1 |a - a_{desired}| + w_2 |h - h_{desired}| + w_3 |k - k_{desired}| + w_4 |p - p_{desired}| + w_5 |q - q_{desired}| + w_6 |H - 1.0| \quad (8)$$

The information in Table 3 summarizes the search specifics and cases explored in the Results and Discussion section. An explanation of how we bypass this issue using visual steering is covered in the next section.

**Table 3: Summary of Explored Cases**

<b>Constant Acceleration</b>	
<i>Search Range:</i>	<i>Objective:</i>
±10% of Table 1	Explore decision space immediately surrounding known optimal solution listed in Table 1 over a wider spectrum than Reference [14] and identify other optimal or near optimal solutions, if any, within each search range.
±25% of Table 1	
±50% of Table 1	
±500% of Table 1	

## RESULTS AND DISCUSSION

### Optimal Solution Acquisition via Visual Steering

One of the many goals of the ATSV is to use an engineer's intuition and/or knowledge gained from prior experience with a particular engineering problem in order to enhance search. As with any model implementation using the ATSV, over the many hours of sampling the design space, the most productive visual steering commands were constantly refined as problem-specific wisdom was gained. The most effective technique found for this problem formulation can be described by the flow chart in Fig. 1.

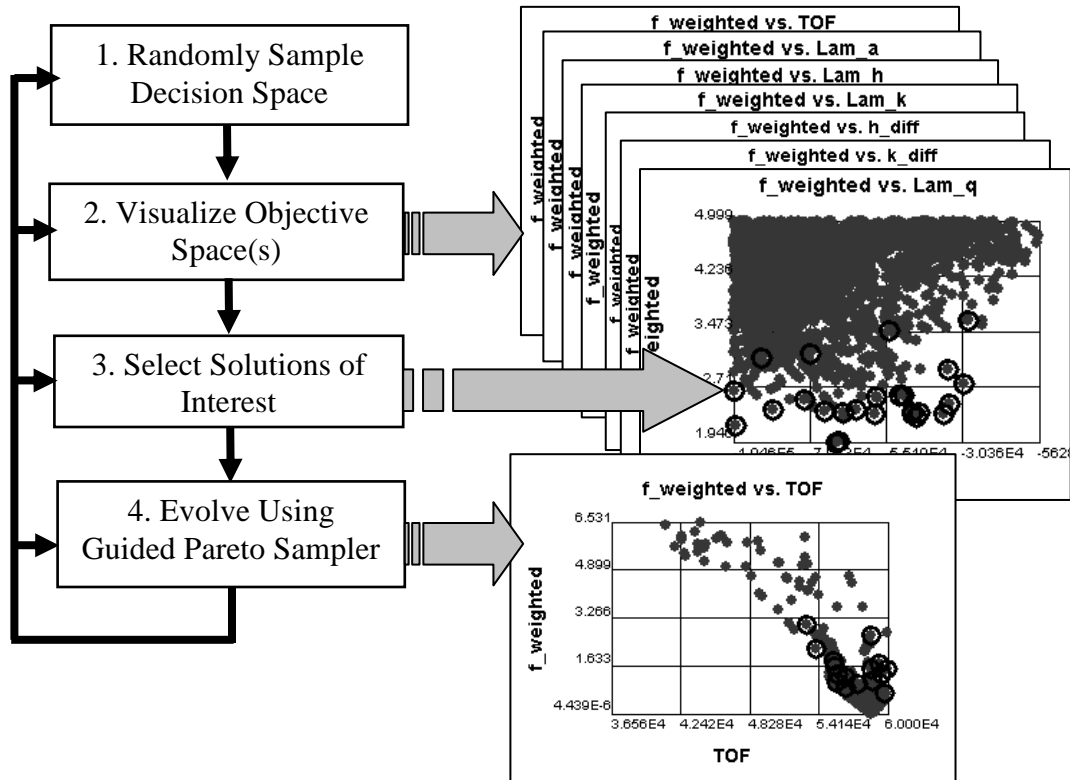


**Fig. 1: Optimal Solution Acquisition via Visual Steering Flow Chart**

First, the decision space is sampled randomly and uniformly anywhere from 100,000 to 1,000,000 times. The objective and decision spaces are then visualized in a variety of combinations using the ATSV's Scatter Plots. The visualization of  $f$  vs. TOF,  $\lambda_{a,o}$ ,  $\lambda_{h,o}$ ,

$\lambda_{k,o}$ ,  $|a-a_{desired}|$ ,  $|h-h_{desired}|$  etc. reveals promising solutions that exist from the randomly sampled set. Solutions of interest are then selected and the exploration of the design space is driven by the Guided Pareto Sampler.

The selection of “solutions of interest” is a problem-specific and designer-specific process that can be difficult to quantify because it relies on abstract information such as a designer’s intuition, knowledge, and/or problem-specific wisdom. Generally, solutions which have small  $f$  are chosen to guide evolutions in early iterations of the exploration process. The selection of solutions used to “guide” evolutions away from pre-convergence is somewhat more difficult to quantify, but a general guideline of the process used for this work is as follows.

Because of the size of the decision space, evolutions often converge to false optima, meaning the progress of solution evolution will halt with  $f \gg 0$ . Pre-convergence issues may also arise from improper weighting of the terms comprising the definition of  $f$ . If this occurs, some or all of the steps listed in Fig. 1 are revisited until  $f$  approaches zero or it is determined, by user insight, that no solution can be found within the given decision space range and the process is terminated. In order to overcome pre-convergence, a diverse selection of points is chosen to guide the evolution. Generally, we choose a variety of promising solutions by examining which terms in  $f$  are lagging in the evolution process. An example of promising solution selection using this technique is illustrated in the three scatter plots shown in Fig. 2. In this example,  $|h-h_{desired}|$ ,  $|k-k_{desired}|$ , and  $|p-p_{desired}|$  are “lagging” after an evolution has pre-converged, meaning their magnitudes are much greater than the other terms comprising  $f$ . As shown, we select points which simultaneously minimize  $f$  and these lagging terms to guide the next evolution. This

technique of guiding the search with lagging terms is simplified for the purposes of demonstration in Fig. 2. The solutions comprising a single guided generation often include the best known solution, lagging term solutions, as well as a healthy set (about 50%) of random solutions within a full or narrowed spectrum decision space. By visually steering the trade space with the ATSV, we can effectively locate optimal solutions without tediously fine-tuning the weights on specific objectives.

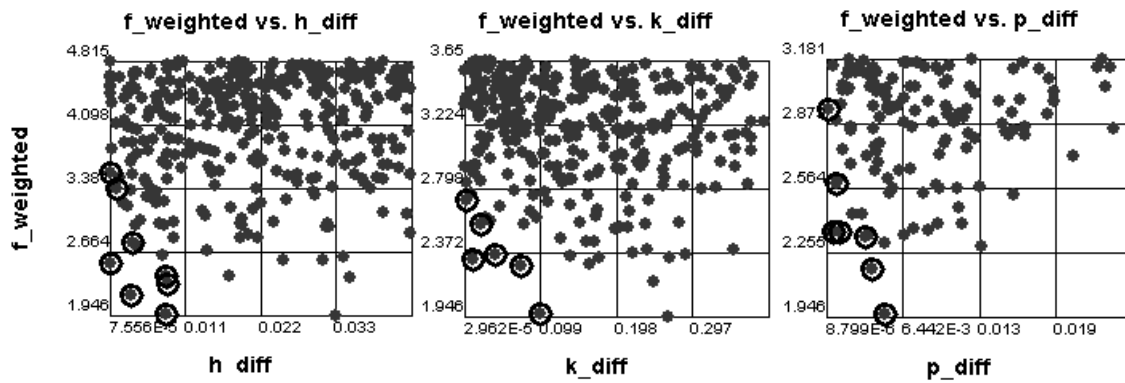


**Fig. 2: Example Selection of Solutions of Interest used to Guide the Next Evolution**

The Guided Pareto Sampler’s ability to pause, adjust, and alter an evolution can drastically increase the effectiveness of evolutionary search. Fig. 3 (a)-(f) shows the progression of many Guided Pareto searches toward optimality over many iterations of the technique described by Fig. 1. Each plot shows  $f$  vs. time of flight, and the solutions chosen to guide a particular evolution are highlighted by black circles. Using this method, the progression toward false optima, where  $f$ ’s approach towards zero is halted, as shown in Fig. 3 (b) and (d), is easily overcome. With a combination of visualization, evolutionary search, and intuition/knowledge inspired adjustments, we are able to visually “steer” solutions toward optimality in order to obtain minimum-time, minimum-

fuel, constant acceleration, or constant thrust orbit transfers (note that minimum-time and minimum-fuel transfers are the same if there are no coast arcs allowed).

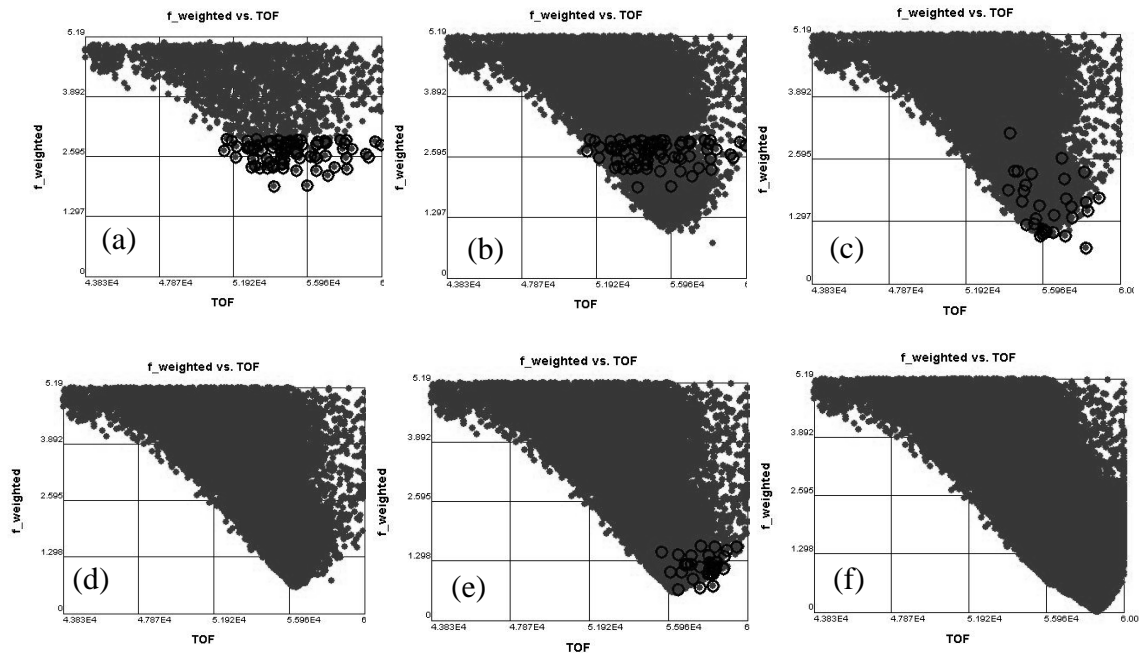


**Fig. 3: Progression of a Typical Search Using the Guided Pareto Sampler**

In order to quantify the point at which the minimization of  $f$  is sufficient for optimality, the final state of the solution explored in the next section (listed in Table 5) is shown in Table 4. In general, solutions which have  $f$  on the order of an arbitrarily chosen tolerance of  $1 \times 10^{-5}$  or less are considered optimal, and the values of the final state of the classical elements in this table are a good measure of the accuracy of all optimal solutions presented in this work.

**Table 4: Typical Optimal Final Classical State**

	Goal	Sufficiently Optimal
$a_{desired}$	42000 (km)	42000 (km)
$e_{desired}$	0.001	0.000999677
$i_{desired}$	1°	0.99999726°
$\Omega_{desired}$	0°	9.76092E-05°
$\omega_{desired}$	0°	0.010314043°
$\theta_{desired}$	Free	Free
$H$	1.0	0.999999
$f$	0	$4.44 \times 10^{-6}$

**Constant Acceleration**

Within the decision space search ranges of  $\pm 10\%$ ,  $\pm 25\%$ , and  $\pm 50\%$  of the known optimal solution listed in Table 1, each evolution process converged toward this known solution. For the  $\pm 500\%$  search range, some evolutions converged toward the solution listed in Table 1 and others converged to a solution which the author considers to be clearly distinct. This “near optimal” solution and a comparison with the optimal solution found in Reference [13] are shown in Table 5. Although only two of the six elements of  $\bar{\lambda}_o$  converge to within 1% of the values listed in Table 1, the time of flight for the near optimal solution is only 0.007% greater. Furthermore, the time history of the classical orbital elements and the thrust vector control angles are almost identical when compared to corresponding time histories for the solution listed in Table 1, as shown in Fig. 4 and Fig. 5. Moreover, trends of  $a$ ,  $i$ ,  $e$ ,  $\alpha$ , and  $\beta$  with time closely match the time history behavior from References [13] and [14].

The assumption that  $\lambda_{h,o}$  and  $\lambda_{p,o}$  are less sensitive than the other initial adjoint variables to the solution quality may be fair, but the idea that these variables are largely

insensitive is not. Upon replacing the value of  $\lambda_{h,o}$  for the optimal set listed in Table 5 with the optimal value from Reference [13], which we will call  $\lambda_{h,o}^{[13]}$ , the value of  $f$  increases by five orders of magnitude. Similar behavior is evident when applying this test for  $\lambda_{p,o}$ ,  $\lambda_{h,o}$  and  $\lambda_{p,o}$  simultaneously, and various randomly chosen values between  $[\lambda_{p,o} \lambda_{p,o}^{[13]}]$  and  $[\lambda_{h,o} \lambda_{h,o}^{[13]}]$ .

**Table 5: “Near Optimal” Adjoint Variable Initial Conditions for Constant Acceleration LEO to GEO Transfer**

$\bar{\lambda}_o$	Optimal Value	% Difference from Reference [13]
$\lambda_{a,o}$ (sec/km)	1.278695	1.445%
$\lambda_{h,o}$ (sec)	590.5856	52.779%
$\lambda_{k,o}$ (sec)	-9333.9	-0.579%
$\lambda_{p,o}$ (sec)	-3397.12	-49.184%
$\lambda_{q,o}$ (sec)	-17526.5	-0.552%
$\lambda_{L,o}$ (sec/rad)	503.6537	2.307%
TOF (sec)	58628.61	0.007%

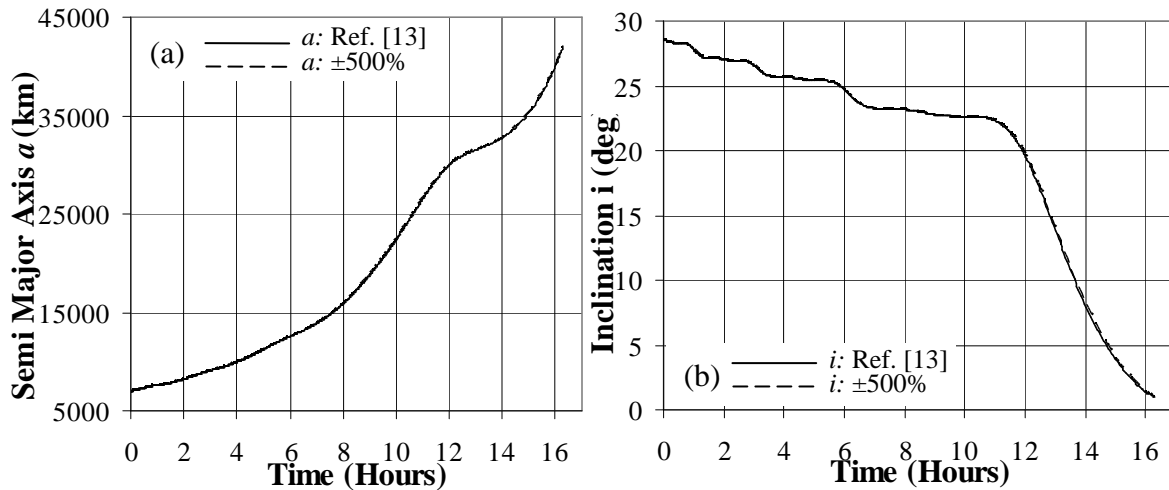


**Fig. 4: (a) Semi-Major Axis and (b) Inclination as a Function of Time for Optimal Trajectory found within  $\pm 500\%$  of Reference [13]**

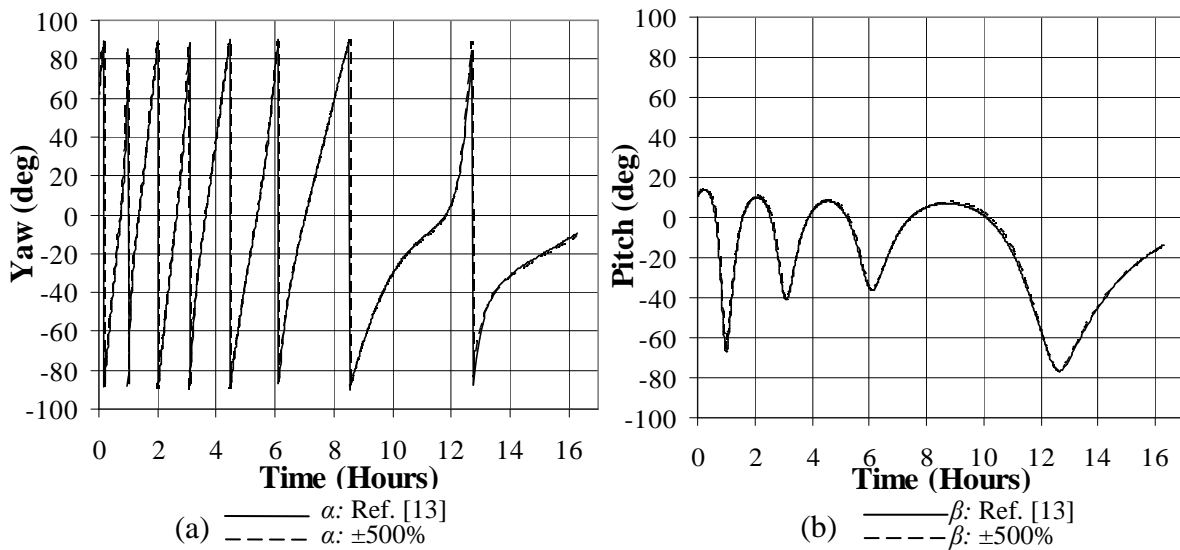


**Fig. 5: Yaw  $\alpha$  and Pitch  $\beta$  as a Function of Time for Optimal Trajectory found within  $\pm 500\%$  of Reference [13]**

The existence of a near optimal solution is intriguing, and implies that there are multiple distinct sets of adjoint variable initial conditions which lead to nearly the same behavior of the orbital elements with time. Accordingly, the concept of “optimality” as referred to in this work should be considered near-optimal, and not truly mathematically optimal.

## SUMMARY AND CONCLUSIONS

ATSV is an effective solution visualization and exploration tool for the constant acceleration LEO to GEO transfer discussed in this work. The “human-in-the-loop” capabilities provided by the ATSV’s sampling techniques, the Guided Pareto Sampler in particular, played an integral role in the efficient acquisition of optimal trajectories. Within a  $\pm 50\%$  search of a known optimal solution, evolutionary search converged toward this solution. The  $\pm 500\%$  search revealed the presence of a clearly distinct near-optimal set of adjoint variable initial conditions, which result in very similar time

histories of the classical orbital elements when compared with a known optimal trajectory.

Any extended work on this topic should consider the search of an even wider spectrum of decision variables for the constant acceleration problem formulation. More sensitivity cases might provide further insight into the relationship between the adjoint variable initial conditions and the time histories of the classical orbital elements and thrust control angles. The sensitivity of optimal trajectories to perturbations in the final desired orbit could be investigated as well. In the interest of model accuracy and actual applicability, the addition of  $J_2$  effects to the system dynamics as well as constraints on the final true anomaly could be added to the problem formulation. Since most of these ideas increase the difficulty of search, in order to implement these ideas in a reasonable time frame, the designer would benefit from the use of distributed and/or cluster computing. With this in mind, the ATSV software development team is currently prototyping a software addition to integrate the power of parallel computing with the effectiveness of “human-in-the-loop” optimization.

## **ACKNOWLEDGMENTS**

This work was supported by the National Science Foundation under Grant No. CMMI-0620948. Any opinions, findings, and conclusions or recommendations presented in this paper are those of the authors and do not necessarily reflect the views of the National Science Foundation.

## **REFERENCES**

- [1] Soelberg, P. O., 1967, “Unprogrammed Decision Making,” *Industrial Management Review*, 8, 19-29.

- [2] Savage, L., 1954, *Foundations of Statistics*. New York, John Wiley & Son.
- [3] Messac, A. and Chen, X., 2000, "Visualizing the Optimization Process in Real-Time Using Physical Programming," *Engineering Optimization*, 32(6), 721-747.
- [4] Ng, W. Y., 1991, "Generalized Computer-Aided Design System: A Multiobjective Approach," *Computer-Aided Design*, 23(8), 548-553.
- [5] Eddy, W. F. and Mockus, A., 1995, "Dynamic Visualization in Modeling and Optimization of Ill-Defined Problems: Case Studies and Generalizations," *Technical Report*, Department of Statistics, Carnegie Mellon University, Pittsburgh, PA.
- [6] Carlsen, D. E., 2008, "Assessment of User-Guided Visual Steering Commands During Trade Space Exploration," *Master's Thesis*, Department of Mechanical & Nuclear Engineering. The Pennsylvania State University, University Park, PA.
- [7] Stump, G., Yukish, M. and Simpson, T. W., 2004, "The ARL Trade Space Visualizer: An Engineering Decision-Making Tool," *10th AIAA/ISSMO Multidisciplinary Analysis and Optimization Conference*, Albany, NY, AIAA, AIAA-2004-4568.
- [8] Jordan, D. D., Spencer, D. B., Simpson, T. W., Yukish, M. A., and Stump, G. M. 2008. "Optimal Spacecraft Trajectories via Visual Trade Space Exploration" *18<sup>th</sup> AAS/AIAA Spaceflight Mechanics Meeting*. Galveston, TX. AAS 08-246.
- [9] Stump, G., S. Lego, M. Yukish, T.W. Simpson and J.A. Donndelinger, "Visual Steering Commands for Trade Space Exploration: User-Guided Sampling with Example", *ASME Design Engineering Technical Conferences - Design Automation Conference*, Las Vegas, NV, ASME, DETC2007/DAC-34684, 2007.

- [10] Price, R. Storn and J. Lampinen, *Differential Evolution - A Practical Approach to Global Optimization*, Berlin, Springer, 2005.
- [11] Kechichian, J. A., “Equinoctial Orbit Elements: Applications to Optimal Transfer Problems” AIAA-90-2976, AIAA/AAS Astrodynamics Conference, Portland, OR, August, 1990
- [12] Edelbaum, T. N., Sackett, L. L., and Malchow, H. L., “Optimal Low Thrust Geocentric Transfer,” AIAA Paper 73-1074, Nov. 1973.
- [13] Kechichian, J. A., “Optimal Low-Earth-Orbit-Geostationary-Earth-Orbit Intermediate Acceleration Orbit Transfer” *Journal of Guidance, Control, and Dynamics*, Vol. 20, No. 4, 1997, pp. 803-811.
- [14] Igarashi, J. *Optimal Continuous Thrust Orbit Transfer Using Evolutionary Algorithms*. M. S. Thesis, The Pennsylvania State University, 2004.